# High-power, null-type, inverted pendulum thrust stand

Kunning G. Xu and Mitchell L. R. Walker
*Department of Aerospace Engineering, High-Power Electric Propulsion Laboratory, Georgia Institute of Technology, College of Engineering, Atlanta, Georgia 30332, USA*

(Received 21 January 2009; accepted 7 April 2009; published online 6 May 2009)

This article presents the theory and operation of a null-type, inverted pendulum thrust stand. The thrust stand design supports thrusters having a total mass up to 250 kg and measures thrust over a range of 1 mN to 5 N. The design uses a conventional inverted pendulum to increase sensitivity, coupled with a null-type feature to eliminate thrust alignment error due to deflection of thrust. The thrust stand position serves as the input to the null-circuit feedback control system and the output is the current to an electromagnetic actuator. Mechanical oscillations are actively damped with an electromagnetic damper. A closed-loop inclination system levels the stand while an active cooling system minimizes thermal effects. The thrust stand incorporates an *in situ* calibration rig. The thrust of a 3.4 kW Hall thruster is measured for thrust levels up to 230 mN. The uncertainty of the thrust measurements in this experiment is $\pm 0.6\%$, determined by examination of the hysteresis, drift of the zero offset and calibration slope variation. © *2009 American Institute of Physics.*
[DOI: 10.1063/1.3125626]

## I. INTRODUCTION

The use of electric propulsion (EP) in space applications has seen enormous growth in the past decade with use on satellites such as DAWN, Deep Space 1, Smart-1, and Hayabusa.[1–4] Recent advances in solar array technology has made on-orbit levels of tens of kilowatts of power possible.[5] Recent mission studies have also highlighted the advantages of using high-power EP for moon and Mars missions to shorten the trip times and maximize delivered payload.[5] Thus, future missions will utilize advanced high-power, high thrust EP devices. In response to this need, a null-type, inverted pendulum thrust stand is constructed and tested to measure the thrust of high-power EP devices.

There are three different pendulum thrust stand configurations: hanging,[6] inverted,[7] and torsional.[8] The hanging pendulum is the simplest of the three and is highly stable due to gravity. However, to achieve the sensitivity levels required for EP would result in pendulum arm lengths that are too large for most vacuum chambers. The torsional configuration provides high sensitivity and allows the restoring force to be independent of the thruster weight because the rotation axis is parallel to the gravity vector. Again, the size and placement of the arms make placement difficult for a limited size vacuum chamber. The inverted pendulum configuration is unstable, but possesses a wide range of sensitivity depending on the stiffness of the flexures and load spring. The inverted pendulum has been used to measure the thrust of a wide range of EP devices, including resistojets,[9] arcjets,[10] magnetoplasmadynamic thrusters,[7] and Hall thrusters.[11] The disadvantage of the inverted pendulum is that the stability and sensitivity are a strong function of flexure stiffness, which is affected by external factors such as temperature and external vibrations. The inverted pendulum thrust stand in this article compensates for vibrations with a damper. The nullification coil holds the thrust stand nearly stationary throughout the testing, which eliminates thrust elevation effects and reduces mechanical oscillations. A multiloop cooling system minimizes thermal effects to help ensure accurate measurements.

Section II presents the details of the thrust stand design. Section III describes the experimental facilities and the thruster. Section IV presents the experimental data and results from operation of the thrust stand. Finally, Sec. V summarizes the findings on the accuracy and repeatability of the thrust stand.

## II. THRUST STAND SYSTEM

Figure 1 is a schematic of the null-type, inverted pendulum thrust stand of NASA Glenn Research Center design.[7] The figure shows all of the major components of the system. The upper motion plate, lower fixed plate, flexures, load spring, null coil, damper coil, and inclination arm are labeled on the drawing. The stand is constructed primarily from aluminum. The novelty of the null-type thrust stand is that it holds the thrust stand in a nearly stationary position at all thrust levels, which eliminates changes in the elevation angle of the thrust vector and reduces error in the thrust measurement. This is achieved with an electromagnetic actuator that counters the thrust created by the thruster in order to maintain zero relative motion of the highly sensitive pendulum. The thrust produced by the thruster is directly correlated with the amount of current required by the electromagnetic actuator to balance the thrust. The thrust stand control system consists of two proportional, integral, derivative (PID) control loops to drive the electromagnetic actuators, one for the damper coil to remove oscillations and one for the null coil. The input for the control loops is a position signal from a Linear Variable Differential Transformer (LVDT) A third PID loop drives a piezoelectric stack for inclination control. The load spring is used to adjust the system spring constant, which allows the user to adjust the required restoring force as

 

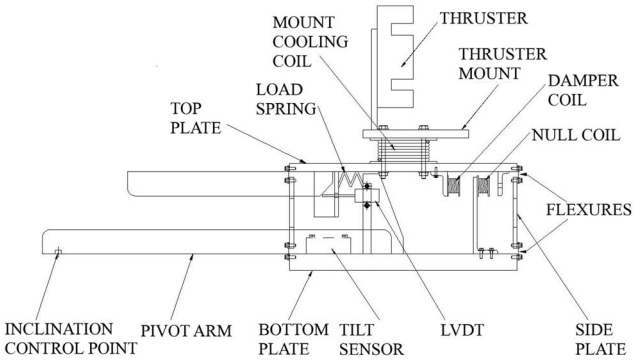


FIG. 1. Schematic of the null-type, inverted pendulum thrust stand.

thruster mass and thrust changes. The following subsections describe each of the thrust stand subsystems in detail.

### A. Inverted pendulum system

The flexures of the stand, along with the load spring, determine the amount of deflection the upper motion plate undergoes for a given applied force. They also determine the maximum mass that can be safely tested on the thrust stand, which is based on their buckling strength. The flexures on this stand are made with extra stiffness to accommodate a mass of approximately 250 kg. There are a total of eight flexures located at the four corners of the stand, with four flexures on the top and bottom plates. The flexures are thin rectangular steel strips attached such that the stand primarily deflects forward and backward. During operation a mounted thruster, as shown in Fig. 1, would produce a thrust vector pointing aft, left in the figure, which causes a backward deflection of the stand. In a normal inverted pendulum, temperature changes can change the stiffness of the flexures, which would affect measurement accuracy.

The load spring and the applied load determine the stable position of the system. It also accommodates for changes in thruster mass and center of gravity. A stiffer spring makes the system more stable and can accommodate larger loads. The load spring is composed of a thin metal band formed into an "M" shape, as shown in Fig. 2. This shape is chosen over a "V" shape to reduce the bending moments at the anchor points. Bending at screw-held flexures typically cause tiny frictional slippage, which result in hysteresis. The two length constants for the spring, $a$ and $b$, are shown in Fig. 2. The "M" shape is a composite of six simple cantilevered beams. The rotation angle for a single cantilevered beam is

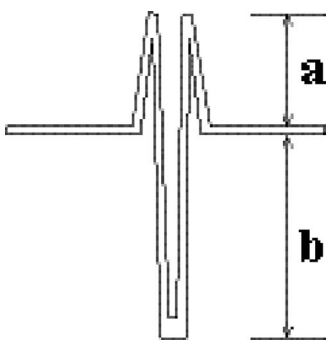


FIG. 2. "M" load spring.

$$\theta = \frac{P\sqrt{L}}{2EI}, \tag{1}$$

where $\theta$ is the rotation angle, $P$ is the thrust force, $L$ is the beam length, $E$ is the elastic modulus, and $I$ is the area moment of inertia. Selecting $a$ and $b$ such that all rotation angles cancel gives

$$2\sqrt{a} = \sqrt{b}. \tag{2}$$

Solving for $b$ results in[12]

$$b = a\sqrt{2}. \tag{3}$$

Using this length ratio, bending moments cancel. The deflection of the spring can be calculated using the deflection for a simple cantilever beam and adding the six pieces of the spring together,

$$d(a) = \frac{Pa^3}{3EI}, \tag{4}$$

where $d(a)$ is the beam deflection as a function of the length of $a$. The total deflection of the spring is a sum of the individual legs. Using Eq. (3), the length $b$ can be replaced with $\sqrt{2}a$ to get

$$d_{\text{total}} = 4d(a) + 2d(1.41a), \tag{5}$$

$$d_{\text{total}} = 4\left(\frac{Pa^3}{3EI}\right) + 2\left[\frac{P(1.41a)\text{^}3}{3EI}\right], \tag{6}$$

$$d_{\text{total}} = 3.22\frac{Pa^3}{EI}. \tag{7}$$

Knowing the total deflection, the spring constant $k$ becomes

$$k = \frac{P}{d}. \tag{8}$$

The overall deflection sensitivity $D$ of an inverted pendulum stand is given by Haag in Ref. 7,

$$D = \frac{P}{(k - mg/R)}. \tag{9}$$

As the spring constant $k$ approaches $mg/R$, the deflection increases to infinity. At high spring constants the deflection is smaller, however noise becomes a larger issue and the system has decreased LVDT resolution. At lower spring constants, the deflections are larger and noise a smaller concern, but the deflections may be too large and outside the LVDT measurement range. The value of $k$ is thus important for successful use of the system as it dictates the sensitivity and displacement range.[7]

### B. Displacement sensing

The displacement of the top plate is measured with a Schaevitz Sensors 100 HR LVDT. The signal is sent through

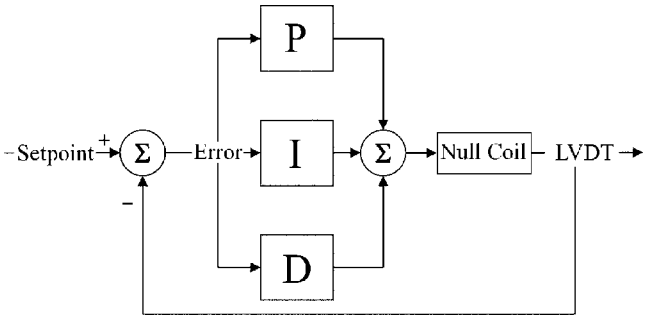


FIG. 3. PID control diagram.

a Schaevitz Sensors ATA-2001 Amplifier. The LVDT has a nominal range of ±2.54 mm with a sensitivity of 4.2 mV per 0.0254 mm.

### C. Thermal control

The thrust stand is actively cooled by a 1100 W VWR International 1173-P refrigerated recirculation chiller in order to maintain thermal equilibrium at all thruster operating conditions. The thrust stand cooling consists of three parallel cooling circuits that travel through the structure, the null coil, and the outer radiation shroud. The top motion plate and lower base plate are actively cooled to minimize error due to flexure thermal effects. The cooling water temperature is monitored by the chiller and never increases by more than 5 °C over the thruster-off condition.

### D. PID control loop

A Stanford Research Systems SIM960 PID controller is used to provide response control through feedback loops using the LVDT as the sensor and the null coil as the control. A diagram of the control loop is shown in Fig. 3, where P, I, and D are the proportional, integral, and derivative controls, respectively.

The three controller gains allow the thrust stand to be tuned specifically for each experimental setup. The proportional control provides a force proportional to the error between the specified location and current location in an attempt to bring the error to zero. As the thruster size and thrust level increases for a fixed spring constant, larger proportional control is needed to counter the deflection. The integral portion provides control relative to the change in error over time. With only a proportional controller, there will always be a disturbance force as the controller only responds to the existence of error. The integral portion takes into account the error over time and responds to bring the error to zero. The derivative control takes the first derivative of the error to predict future changes and change the controller response time. A larger derivative term improves the response time of the controller to allow for control of smaller oscillations.

The null coil and the damper coil are electromagnetic actuators that reduce thrust stand deflection and reduce mechanical oscillations, respectively. Each electromagnetic actuator is composed of a 3/8 in. (0.9529 cm) diameter samarium-cobalt permanent magnet positioned inside a 9/16 in. (1.43 cm) diameter copper tube. Each copper tube has two 1250-turn 28 gauge copper wire solenoid winding placed on each end, wired in series. The null coil is energized throughout testing, which requires active cooling of the center of the copper tube. Heat dissipating grease is applied between each layer of the solenoid windings to assist with cooling the solenoid. A Trust Automation TA115 amplifier provides the current for the actuation. When actuated, the stationary solenoids apply a force to the permanent magnets, which are attached to the upper plate, and provide the force to balance the thrust vector.

The damper coil is necessary to control oscillations since the inverted pendulum is by design severely under-damped to improve sensitivity. The damper control is a derivative of the LVDT position signal, and the current is provided by a second TA115 amplifier. This creates an effect similar to natural dampers, such as water or oil dashpots. The strength of the response is controlled by a second SIM960, using a PD control loop so it reacts mainly to changes in velocity.

### E. Inclination control

A leveling system is required to ensure that the thrust vector is perpendicular to the length of the flexures. If the thrust vector is not perpendicular to the flexures, a portion of the thrust will have a vertical component, which will not cause the stand to move, and thus not be measured. A Spectronics RG-33T-544-A-005 tilt sensor monitors the inclination of the thrust stand and a Spectronics MUPI-2 signal module reads the tilt sensor signal. The thrust stand inclination is changed with a geared dc motor (Pittman GM9413–5) and a Piezo Systems, Inc. model TS18-H5–202 piezoelectric stack. The geared dc motor is used to raise and lower the back of the thrust stand on a $\frac{1}{4}$ inch diameter, 80 threads per inch stainless steel threaded rod. A high pitch thread is required to allow for fine height adjustments via the geared motor. Once the stand is adjusted to near-level with the geared motor, the piezoelectric stack is then used to exactly level the system. The piezoelectric stack is controlled by a third SIM960 PID system with a Trust Automation TA320 amplifier using the tilt sensor as the input. The controller varies the voltage applied to the stack in order to raise or lower the stand to maintain level. The piezoelectric stack has a displacement of 14.5 $\mu$m ± 2 $\mu$m.

### F. Calibration method

A remotely controlled geared motor-driven pulley system is employed to provide *in situ* thrust stand calibration by loading and off-loading small weights to simulate thrust before and after each test point. Upon command, the motor deploys small weights to sequentially apply a known force in the direction of the thrust vector. In response, the null coil controller applies a current through the null coil to counteract this force. A linear curve-fit of null-coil current versus calibrated weight (thrust) is then obtained and used for thrust measurements.

### G. Thrust stand error

The majority of the sources of error in the thrust stand are of mechanical origins, due to the moving pieces within

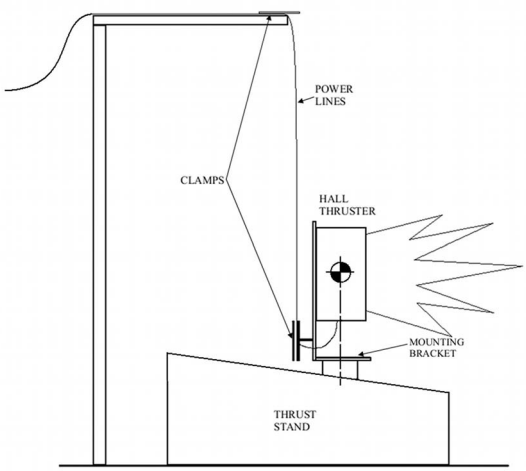


FIG. 4. Waterfall power lines.

the stand. The largest of these are the flexures, load spring, and power wires connecting the thruster. They are subject to minute expansions and contractions over time. The test results show an error of ±0.6% of full-scale calibration. The uncertainty, or error, of the thrust measurements in this paper, determined by examination of the hysteresis and drift of the zero offset and calibration slope, is ±2.3 mN, using a 400 mN calibration weight set.

### H. Thruster power and propellant feeds

The power leads for the thrust stand are mounted in a "waterfall" type fashion as shown in Fig. 4. The layout is designed such that any thermal expansion in the wires will lead to forces in the direction normal to the thrust vector. With four flexures located at the corners of the stand, the stand can only move forward and back, thus only forces parallel to the thrust vector will cause any deflection. Any side to side motions are negligible.

High currents through the power lines cause heating of the conductive wire and thermal drift. The power wires are Mueller Electric 18 AWG Ultra-Flex, which is a stranded copper wire composed of very thin (>28 AWG) strands. This allows for the wire to bend very easily, which minimizes any thermal drift due to expansion from Ohmic heating. It also minimizes drift due to hysteresis. No more than 5 A is passing through each line, to help reduce the effects of Ohmic heating. There was no noticeable thrust generated due to the Ohmic heating.

Propellant line connections are built into the stand and move with the stand so that the lines do not generate hysteresis effects on the measurements. The 1/4 in. (0.635 cm) stainless steel lines from the propellant feedthroughs are connected to the secured thrust stand base via Swagelok bulkhead fittings. Inside the stand, the lines are brought from the base to the pivot arm where they are attached with bulkhead fittings. A set of "C" shaped lines connect the pivot arm lines to the top plate arm. These lines, in addition to feeding propellant, provide a damping effect on the stand motion. From the upper arm, the propellant lines are connected to the thruster.

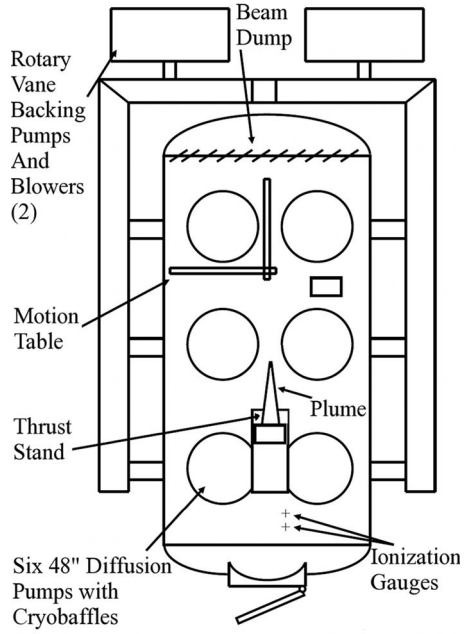


FIG. 5. Schematic of the VTF.

## III. EXPERIMENTAL SETUP

### A. Vacuum facility

All experiments are conducted in the vacuum test facility (VTF), shown schematically in Fig. 5. The VTF is a stainless steel vacuum chamber that has a diameter of 4 m and a length of 7 m. The VTF pumping speed is varied by changing the number of diffusion pumps in operation. The combined pumping speed of the facility is 600 000 l/s on air and 155 000 l/s on xenon with a base pressure of $1.2\times10^{-4}$ Pa ($9.5\times10^{-7}$ Torr).[13] At the anode flow rates investigated—1 to 7 mg/s, and at a nominal xenon pumping speed of 155 kl/s, the operating pressures of the VTF range from $1.3\times10^{-3}$ Pa-Xe ($1.3\times10^{-5}$ Torr-Xe) to $2.6\times10^{-3}$ Pa-Xe ($2.6\times10^{-5}$ Torr-Xe).

Table I shows the VTF operating pressure for each flow rate at the nominal xenon pumping speed of 155 kl/s. The operating pressures are representative of those seen in low Earth orbit. The chamber pressures listed in Table I are the indicated pressures from the nude gauge, corrected for xenon using the measured $N_2$ referenced base pressure and a correction factor of 2.87 for xenon.[14] Chamber pressure is monitored by a Varian model UHV-24 nude gauge with a Varian UHV senTorr Vacuum Gauge Controller. The UHV-24 nude gauge is calibrated for air by the manufacturer. Pressure mea-

TABLE I. VTF operating pressure for given flow rates at a nominal pumping speed of 155 kl/s on Xenon.

| Anode+Cathode Flow Rate (mg/s) | Pressure (Torr-Xe) | Pressure (Pa-Xe) |
|---|---|---|
| 1 | 1.3 e-5 | 1.8 e-3 |
| 3 | 1.6 e-5 | 2.2 e-3 |
| 5 | 2.0 e-5 | 2.6 e-3 |
| 7 | 2.3 e-5 | 3.0 e-3 |

surements are corrected for xenon using the known base pressure on air and a correction factor of 2.87 for xenon according to the following equation:[14]

$$P_c = \frac{P_i - P_b}{2.87} + P_b, \tag{10}$$

where $P_c$ is the corrected pressure on xenon, $P_b$ is the base pressure, and $P_i$ is the indicated pressure when xenon is flowing into the vacuum chamber. The ionization gauge measures pressure over the range of $10^{-2}$ Pa ($10^{-4}$ Torr) to $10^{-10}$ Pa ($10^{-12}$ Torr) with an accuracy of $\pm 20\%$ as reported by Varian.[15]

### B. Hall thruster

All experiments are performed on the Pratt & Whitney T-140 laboratory-model Hall thruster. The T-140 has a mass of approximately 8 kg, mean outer diameter of 143 mm, a channel width of 23 mm, with a nominal thrust of 200 mN at a nominal power rating of 3.4 kW.[16] The discharge channel of the T-140 is made from boron nitride. A Moscow Aviation Institute type $LaB_6$ cathode is located at the 12 o'clock position. The cathode orifice is located approximately 70 mm downstream from the outer front pole piece. The cathode flow rate is set at 1.0 mg/s for all cases investigated. A more detailed description of the T-140 can be found in Ref. 1.

The T-140 and its cathode are operated with five dc power supplies for the inner magnet, outer magnet, anode, cathode extraction electrode, and cathode heater. The thruster electrical connections enter the chamber through separate feedthrough ports. The thruster discharge (anode) supply is connected to a filter consisting of a 1.3 k$\Omega$ resistance in series with the discharge current and a 95 $\mu$F capacitor in parallel. The filter provides isolation of the discharge power supply from the discharge oscillations of the plasma and ensures that any oscillations are not a product of feedback between the power supplies and plasma. Discharge current oscillations are measured with a F.W. Bell IHA-25 Hall effect current sensor connected to a Tektronix TDS 3034B oscilloscope. High-purity (99.9995% pure) xenon propellant is supplied to the Hall thruster from compressed gas bottles through stainless-steel feed lines. MKS 1179JA mass flow controllers meter the anode and cathode propellant flow. The flow controllers are calibrated with a custom apparatus that measures gas pressure and temperature as a function of time in an evacuated chamber of known volume. The mass flow controllers have an accuracy of $\pm 1\%$ full scale.

## IV. EXPERIMENTAL RESULTS

### A. T-140 calibration

Thrust calibration of the null-type inverted pendulum thrust stand is conducted with the method presented earlier, with 0.002 g uncertainty in calibration weight mass. Magnetic tares are measured by passing current through each set of thruster magnet coils and are found to be negligible. Cold flow tares due to cathode-only flow without a discharge are also found to be negligible. This last result is expected since the cathode centerlines are inclined approximately 45° below the horizontal. Anode flow tares are not required because the anode flow is closed throughout the calibration.

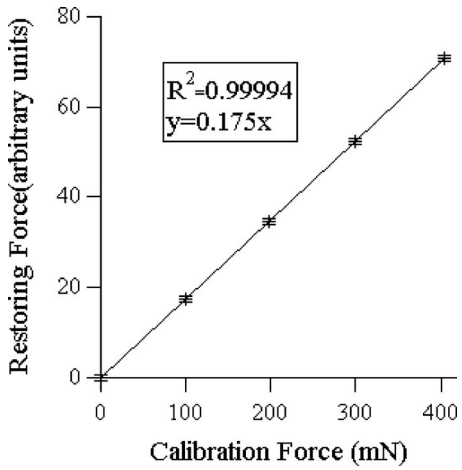


FIG. 6. T-140 thrust stand calibration data.

A calibration curve is taken prior to chamber pump down and thruster firing. Figure 6 shows the calibration data from the experiment in vacuum. The calibration is taken prior to thruster firing, with any necessary subsequent calibrations performed between thruster firings when the thruster is off. We can see from the figure that the thrust stand behaves in a linear fashion as expected. The $R^2$ correlation is very good at 0.999 94 for the linear curve fit with zero $y$-intercept.

### B. Thruster performance data

The thrust stand is allowed to reach thermal equilibrium prior to thrust measurement recording. This typically takes 10 min and is signified by no drift in the null coil current. The first calibration is performed before thruster ignition. Each test point is run for 5 min at minimum to ensure the thruster has reached steady operation. Thermal equilibrium is reached faster during testing because changes in power and thermal conditions between test points are not as large as between thruster off and on.

The thrust is the difference between the nullification current at the test point and the current at zero thrust. The value is then converted to thrust with the most recent calibration equation. After a 30 min test period, approximately 5–6 operating points, the thruster is shut down and the thrust stand allowed to reach zero-thrust steady state. The thrust measurements for each operating condition are plotted in Fig. 7. The figure shows the measured thrust versus discharge voltage at different thruster power levels.

## V. CONCLUSION

A null-type, inverted pendulum thrust stand for high-power EP thrusters has been built and tested. The addition of the null capability to the inverted pendulum design minimizes error due to thrust stand deflections. The thrust stand is cooled from three separate cooling loops. Initial calibration and operation test are performed using a Pratt & Whitney T-140 Hall effect thruster, but the thrust stand is suitable for testing of various other EP devices. The load spring can be

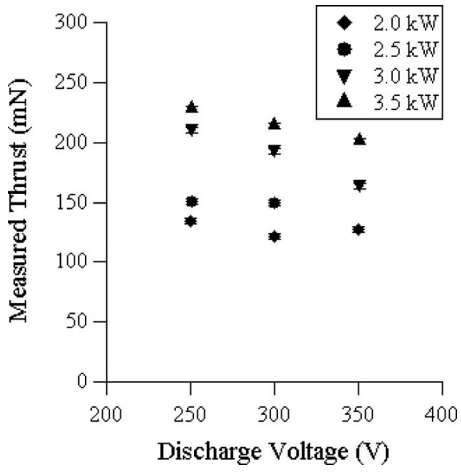


FIG. 7. T-140 thrust measurements.

changed to vary the stiffness of the stand to allow for different thrust levels and thruster masses. The results show a high resolution and error at ±0.6% of full-scale calibration, ±2.3 mN at 400 mN calibration for this experiment.

The performance of the thrust stand is dependant on multiple factors, and to obtain a high level of measurement accuracy, disruptive effects such as thermal expansion, mechanical oscillations, and PID sensitivity must be taken into consideration. The stand is sensitive to small changes in mass or center of gravity of the thruster, and must be adjusted accordingly. Null and damper coil heating can be an issue if too much current is driven, thus care needs to be taken when choosing gains for the PID controllers and the proper load spring.

## ACKNOWLEDGMENTS

The research contained herein was sponsored by the Air Force Research Laboratory. (Dr. James Haas is the contract monitor). The authors would like to thank Dr. Thomas Haag at NASA GRC for the thrust stand drawings, the Georgia Tech Aerospace machine shop for fabrication of the hardware used in the study, Pratt & Whitney for the donation of the T-140 Hall effect thruster and support equipment, and the departmental technical staff and other graduate students at HPEPL for help in maintaining the facilities. Kunning Xu is supported by the National Defense Science and Engineering Graduate Fellowship, and the Georgia Institute of Technology Institute Fellowship. The authors are greatly appreciative of this support.

[1] A. Sengupta, J. A. Ander, C. Garner, and J. R. Brophy, J. Propul. Power **25**, 105 (2009).
[2] G. D. Racca, A. Marini, L. Stagnar, and J. van Dooren, Planet. Space Sci. **50**, 1323 (2002).
[3] J. R. Brophy, G. B. Ganapathi, and C. Garner, Proceedings of the 40th Joint Propulsion Conference and Exhibit, Fort Lauderdale, FL, July 2004 (unpublished).
[4] H. Kuninaka, K. Nishiyama, and I. Funaki, Proceedings of the 42nd Joint Propulsion Conference and Exhibit, Sacramento, CA, July 2006 (unpublished).
[5] R. H. Frisbee, Proceedings of the 42nd Joint Propulsion Conference and Exhibit, Sacramento, CA, July 2006 (unpublished).
[6] K. A. Polzin, T. E. Markusic, and B. J. Stanojev, Rev. Sci. Instrum. **77**, 105108 (2006).
[7] T. W. Haag, Rev. Sci. Instrum. **62**, 1186 (1991).
[8] T. W. Haag, Rev. Sci. Instrum. **68**, 2060 (1997).
[9] D. M. Gibbon, M. F. Paul, and T. Lawrence, Proceedings of the 36th Joint Propulsion Conference and Exhibit, Huntsville, AL, July 2000 (unpublished).
[10] Q. E. Walker, W. Hargus, and M. A. Cappelli, Proceedings of the 34th Joint Propulsion Conference and Exhibit, Cleveland, OH, July 1998 (unpublished).
[11] D. H. Manzella, R. S. Jankovsky, and R. R. Hofer, Proceedings of the 38th Joint Propulsion Conference and Exhibit, Indianapolis, IN, July 2002 (unpublished).
[12] T. W. Haag, personal communications (2009).
[13] D. Palmer and M. Walker, Proceedings of the 44th Joint Propulsion Conference and Exhibit, Hartford, CT, July 2008 (unpublished).
[14] S. Dushman, *Scientific Foundations of Vacuum Technique* (Wiley, New York, 1958), Vol. 4.
[15] Varian Inc., Vacuum Measurement Catalog, accessed 2009 April 25. Available from URL: http://www.variance.com/image/vimage/docs/products/vacuum/measure/shared/measure-catalog.pdf.
[16] C. H. Mclean and J. B. McVey, Proceedings of the 35th Joint Propulsion Conference and Exhibit, Los Angeles, CA, June 1999 (unpublished).